Research Article

Melek Karaaslan, Nuran Gokdere, Batuhan Ozturk, Basar Karaca, Mehmet Bay, Suzan Biran Ay, Aslı Koc, Arzu Z. Karabay, Mujde Eryılmaz, Nihan Kosku Perkgoz, Hayriye G. Saltan Iscan and Ismail M. Palabıyık*

Synthesis, characterization and biological activity of metal nanoparticles with green method using apple industry waste

https://doi.org/10.1515/ntrev-2025-0281
Received September 5, 2025; accepted January 30, 2026; published online March 2, 2026

Abstract: Apple is one of the four most produced fruits in the world. The remaining pulp from production accounts for over 25 % of the processed fruit. Apple pulp and peel contain phenolic compounds such as flavonoids and flavonoid glycosides, making them a potential candidate for green nanoparticle synthesis. Green synthesis refers to the production of nanoparticles through a process that utilizes a natural molecule and metal salts as reducing agents. In this study, metal nanoparticles were synthesized using an extract prepared from apple pomace waste via green synthesis. The synthesized nanoparticles were characterized using UV–visible spectroscopy, Raman, optical microscopy, energy-dispersive X-ray, atomic force microscopy, and scanning electron microscope. The antibacterial, antibiofilm, antiquorum sensing, and anticancer activities of the synthesized nanoparticles were then investigated. According to the antibacterial activity results, the best activity was seen with silver nanoparticles against *Staphylococcus epidermidis* ATCC 12228 with 15.625 µg/mL. Similarly, the best antibiofilm activity was seen with silver nanoparticles. However, significant biofilm inhibition was seen with zinc nanoparticles, tin nanoparticles, and cobalt nanoparticles at higher concentrations. Anticancer activity was studied in six different cell lines: HCT-116 and SW480 colon cancer cell lines, A549 and H1975 lung cancer cell lines, and A2780 and OVCAR3 ovarian cancer cell lines. The best activity was shown with nickel nanoparticles.

Keywords: apple pomace; green synthesis; biological activity

***Corresponding author: Ismail M. Palabıyık**, Department of Analytical Chemistry, Faculty of Pharmacy, Ankara University, Ankara, Türkiye, E-mail: mpala@pharmacy.ankara.edu.tr
Melek Karaaslan and Hayriye G. Saltan Iscan, Department of Pharmacognosy, Faculty of Pharmacy, Ankara University, Ankara, Türkiye
Nuran Gokdere, Department of Analytical Chemistry, Faculty of Pharmacy, Ankara University, Ankara, Türkiye; and Graduate School of Health Sciences, Ankara University, Ankara, Türkiye
Batuhan Ozturk, Department of Analytical Chemistry, Faculty of Pharmacy, Ankara University, Ankara, Türkiye; Graduate School of Health Sciences, Ankara University, Ankara, Türkiye; and Department of Analytical Chemistry, Faculty of Pharmacy, Ankara Medipol University, Ankara, Türkiye. https://orcid.org/0000-0002-3619-7138
Basar Karaca, Microbiology Research Laboratory, Department of Biology, Faculty of Science, Ankara University, Ankara, Türkiye
Mehmet Bay, Department of Electronics and Automation, Vocational School of Information Technologies, Eskisehir Technical University, Eskisehir, Türkiye. https://orcid.org/0000-0001-6447-6460
Suzan Biran Ay, Department of Chemical Engineering, Faculty of Engineering, Eskisehir Technical University, Eskisehir, Türkiye. https://orcid.org/0000-0002-2968-4982
Aslı Koc and Arzu Z. Karabay, Departmant of Biochemistry, Faculty of Pharmacy, Ankara University, Ankara, Türkiye. https://orcid.org/0000-0002-2482-0359 (A.Z. Karabay)
Mujde Eryılmaz, Department of Pharmaceutical Microbiology, Faculty of Pharmacy, Acibadem Mehmet Ali Aydinlar University, İstanbul, Türkiye
Nihan Kosku Perkgoz, Department of Electrical and Electronics Engineering, Faculty of Engineering, Eskisehir Technical University, Eskisehir, Türkiye. https://orcid.org/0000-0003-1331-0959

1 Introduction

Apple (*Malus domestica* (Suckow) Borkh.) is of great importance for the agricultural economy and one of the four most produced fruits globally [1, 2]. According to the Food and Agriculture Organisation (FAO), worldwide production reached 93.1 million metric tonnes by 2021, with Turkey, Italy and France being among the largest producing countries [2, 3]. Although most apples are consumed fresh, nearly one-third are processed into high value-added products such as juice, cider, canned apples, dried fruit, vinegar, and jelly [3, 4]. The pomace left over from the production of the products from apples accounts for more than 25 per cent of the processed fruit and is mainly composed of insoluble components such as peel, core, seeds and stems [4, 5]. Although the

Open Access. © 2026 the author(s), published by De Gruyter. This work is licensed under the Creative Commons Attribution 4.0 International License.

ratios vary depending on factors such as apple variety, maturity, enzyme use, and production steps (e.g., washing and boiling), apple pomace and peel contain dietary fibres like pectin and cellulose, and phenolic compounds including flavonoids, flavonoid glycosides, quinic acid and its derivatives, chalcones, cinnamic and coumaric acids, catechins, and cyanidins [3, 5] Due to this rich content, Zack et al. [6], Vandorou et al. [7] and Pascoalino et al. [8] focused their studies on producing high value-added products from pulp.

In developing countries, the steady increase in population and industrial activities has led to a substantial rise in overall and per capita solid waste generation. This growth, coupled with ongoing economic development, presents significant challenges for waste management systems. Solid waste originating from various human activities – both domestic and industrial – poses considerable risks to public health and the environment if not managed through an integrated and effective solid waste management framework. Biodegradable and non-biodegradable waste streams each present distinct disadvantages and environmental implications. If improperly treated or disposed of, both types of waste can contribute to serious ecological degradation and social harm. Among the sustainable strategies for managing biodegradable waste is its utilization as a raw material for the green synthesis of nanoparticles (NPs). Biomass, as a renewable, abundant, chemically diverse, and cost-effective resource, offers a promising alternative for the production of value-added nanomaterials through environmentally friendly and economically viable methods [9, 10].

Nanotechnology can be defined as the science and engineering that involves design, synthesis, characterization, manipulation and application of functional materials and devices using NPs with dimensions ranging from 1 to 100 nm. There are different physical and chemical methods to successfully synthesize NPs. All these methods have two main approaches that can be applied to any research in the field of nanoscale science. These are top-down and bottom-up synthesis approaches. Each approach has its own characterization and application. In both synthesis techniques, the preparation of NPs involves the use of chemicals that are quite expensive and have a higher probability of damaging the environment and have various toxic effects. In order to eliminate this disadvantage, NPs synthesis using various parts of plants has recently found an important place in scientific research because it is environmentally friendly, biocompatible and stable [11, 12].

NPs synthesized by biological methods are considered as clean, safe, environmentally friendly, cheap and non-toxic methods compared to traditional approaches and are therefore suggested as potential environmentally friendly alternatives compared to chemical and physical approaches. The ability of plants and microorganisms to take up and accumulate metallic ions from their environment makes them potential candidates for the synthesis of nanomaterials. Biological synthesis of NPs is included in the approach called “green synthesis” or “green chemistry” methods, which have recently gained high popularity [12, 13].

Antibiotic resistance is one of the most important problems of our time. Every passing day, bacteria that have become resistant to antibiotics are reported from different parts of the world, and the infections caused by these bacteria, the majority of which are multiresistant, are a significant source of morbidity and mortality. There is an urgent need for new compounds with antibacterial effects in the treatment of infections caused by resistant bacteria. Although researchers have focused their studies on this issue, treatment options that can be effective in solving the resistance problem have not been found today. The failure experienced in this regard and the inevitable development of resistance against existing antibiotics have led scientists to research alternative treatment options [14, 15]. It is predicted that the resistance problem can be overcome by finding molecules that will inhibit the mechanisms that play a role in pathogenicity. The quorum sensing (QS) mechanism is effective in the synthesis of virulence factors that play a role in the pathogenicity of bacteria and in biofilm formation. For this reason, in recent years, studies have focused on molecules with antibiofilm and anti-QS effects that can be used as an alternative to antibacterials in the treatment of bacterial infectious diseases. It is thought that anti-QS and antibiofilm compounds will be effective in controlling the resistance problem [16, 17].

Cancer is the abnormal growth of tissues or cells that exhibit autonomous uncontrolled division, resulting in a progressive increase in the number of cell divisions. It is a significant health problem worldwide, as it causes significant morbidity and mortality. In particular, there are difficulties in the fight against cancer in the development of treatments that target severely proliferating tumors. Chemotherapy is a method used in cancer treatment and has characteristics such as exhibiting low specificity and dose-limiting toxicity [18]. The application of nanotechnology for cancer treatment is mostly based on early tumor detection and diagnosis by nanodevices that have the ability to selectively target and deliver chemotherapeutic drugs to specific tumor sites [19]. NPs are widely used in cancer diagnosis and treatment thanks to their chemical, physical and optical properties. Since NPs with appropriate surface modifications can selectively target tumors, their effects on cancer cell migration or metastasis have attracted the attention of many researchers [20].

The aim of this study is to synthesize, to characterize and investigate the biological activities of metal NPs synthesized using apple waste. For this purpose, extracts were prepared from apple industrial wastes with high phenolic and flavonoid content using different solvents. Metal NPs were synthesized from ethanolic extract with high phenolic content. The characterization of the synthesized NPs were examined using UV–vis (UV–visible) spectroscopy, Raman spectroscopy, optical microscopy, energy dispersive X-ray (EDX) spectroscopy, atomic force microscopy (AFM) and scanning electron microscope (SEM). Then, the antibacterial, antibiofilm, anti-QS and anticancer activities of the synthesized NPs were examined.

2 Materials and methods

2.1 Materials

Apple pomace was provided from a factory (Tunay Gıda Fruit Processing Industry.) in Erzincan, Turkey, which produces organic apple juice, concentrate and puree in 2023. Two types of pomaces were received: one was rich in peels and the other consisted of pulp without peels. All chemicals and reagents used in this study were of analytical grade. Gallic acid, Folin–Ciocalteu reagent, sodium carbonate, silver chloride, zinc chloride, titanium (IV) chloride, cerium (III) acetate, nickel (II) chloride, cobalt (II) chloride, copper (II) chloride, tin (II) chloride, iron (III) chloride, sodium hydroxide, ethanol and other solvents were purchased from Sigma-Aldrich. MTT was purchased from Carl Roth. RPMI medium, fetal bovine serum, penicillin/streptomycin, and L-glutamine were purchased from Capricorn.

Characterization techniques were performed as follows: optical microscopy (Nikon Eclipse LV100NDA) for surface observation, X-ray diffraction (Rigaku MiniFlex 600) for crystal structure analysis, SEM (ZEISS Supra 50V) for surface morphology, EDX (Oxford INCA Energy) for elemental composition, Raman spectroscopy (WITec alpha-300R) for molecular vibrations, and AFM (NanoMagnetics ezAFM™) for surface topography, Spectroscopic measurements were performed using a Shimadzu 1,601 model dual-beam spectrophotometer (Kyoto, Japan). For the incubation process, a Lab Comparation SIF500R (Seoul, South Korea) model incubator shaker was used. For the centrifuge, a Nüve NF200 (Ankara, Turkey) model centrifuge was used. For pH measurement, an ISOLAB Laborgeräte GmbH (Eschau, Germany) digital pH meter was used. The mixing process was performed using an ISOLAB Laborgeräte GmbH (Eschau, Germany) magnetic stirrer. The weighing process was performed using a Shimadzu ATX224 model weighing device (Kyoto, Japan). Thermo, Multiskan Go was used for the microplate reader, Sanyo for the CO2 incubator, Holten for the laminar air, and Olympus for the inverted microscope.

2.2 Extraction

Both pomace types were extracted in 70 % ethanol for 24 h and subjected to ultrasonic extraction for 1 h, then filtered and the filtrate was concentrated. This process was repeated for 10 days, and total extracts (TE1, TE2) were obtained. The phenolic compound content of the total extracts was determined by Folin–Ciocalteu method and the peel-rich extract with the highest phenol content was selected. This extract (TE2) was subjected to liquid-liquid partitioning and extracted with hexane (HSE) and ethyl acetate (EASE) and the remaining aqueous phase was lyophilised to obtain aqueous sub-extract (ASE).

2.3 Total phenolic content

Total phenolic content of TE1 and TE2 was determined by Folin–Ciocalteu method [21]. 100 µL aqueous extract solution was mixed with 400 µL 10 % Folin–Ciocalteu reagent and 800 µL 5 % sodium carbonate solution, vortexed and incubated at room temperature for 30 min. Absorbance at 765 nm was measured and the results were calculated as mg gallic acid equivalents (GAE)/g dry extract according to the gallic acid calibration curve. The experiments were carried out at least three times.

2.4 Synthesis of NPs

Approximately 3 mg of ethyl acetate sub-extract (EASE) was dissolved in distilled water. Then, 20 mmol of metal salt was added. The pH of the prepared mixture was adjusted to 12 with sodium hydroxide. The solution was incubated at 90 °C for 3 h. The solution that reached room temperature was centrifuged 3 times at 5,000 rpm and the precipitate was dried at 60° [11, 13]. Optimizations of extract amount and incubation time were performed for each NPs.

2.5 Characterization

The characterization process of Ag (silver), Ni (nickel), Co (cobalt), Cu (copper), Fe (iron), Zn (zinc), Ce (cerium), Sn (tin) and Ti(titanium) NPs synthesized with apple extract was carried out using various characterization methods to

evaluate morphology, elemental composition and structural properties. The optical properties of the sample were analyzed using the UV-probe software in 1 cm quartz cuvettes on a Shimadzu 1,601 model dual beam spectrophotometer (Kyoto, Japan). Optical microscopy was used to evaluate homogeneity, growth rate and physical properties. SEM with Gemini Supra 50 VP system provided high resolution images of the surface up to 3,000× magnification. EDX was used to analyze the elemental composition. Raman spectroscopy using a continuous laser at 532 nm wavelength examined molecular vibrations and bond interactions. AFM was used to examine surface topography, roughness and height profiles.

2.6 Antibacterial activity

To evaluate the antibacterial activity of metal NPs (AgNPs, CuNPs, ZnNPs, CoNPs, NiNPs, FeNPs, CeNPs, SnNPs and TiNPs); *Staphylococcus aureus* ATCC 25923, *S. aureus* ATCC 43300 (methicillin-resistant, MRSA), *Bacillus subtilis* ATCC 6633, *Enterococcus faecalis* ATCC 29212 and *Staphylococcus epidermidis* ATCC 12228 (as Gram-positive strains); *Escherichia coli* ATCC 25922, *Pseudomonas aeruginosa* ATCC 27853, *P. aeruginosa* PAO1, *Klebsiella pneumoniae* ATCC 13883 and *Chromobacterium violaceum* ATCC 12472 (as Gram-negative strains) were tested.

The evaluation of antibacterial activity was performed using the broth microdilution method and in full compliance with the Clinical and Laboratory Standards Institute (CLSI) guidelines [22]. The metal NPs used in the study were diluted to concentrations ranging from 2,000 µg/mL to 3.91 µg/mL using the twofold serial dilution method. These dilutions were prepared in Mueller–Hinton Broth (MHB; Difco Laboratories, Detroit, MI, USA). The control wells contained only bacterial inoculum and MHB. The inocula used were obtained from overnight cultures and the final culture suspension in each well of the microtitre plate (LP Italiana, Italy) was adjusted to 5×10^5 CFU/mL. The microtitre plates were incubated at 37 °C for 18–24 h. The minimum inhibitory concentrations (MICs) were defined as the lowest concentrations (µg/mL) of NPs at which visible bacterial growth was completely inhibited. Ciprofloxacin (Sigma, USA) was employed as the reference antibiotic.

2.7 Antibiofilm activity

Prior to the antibiofilm tests, the minimum inhibitory concentrations (MIC) of the metal NPs against the *P. aeruginosa* PAO1 strain were determined. For the dilution procedure, sub-MIC concentrations of each NPs (MIC/2, MIC/4, MIC/8 and MIC/16 with the exception of CeNPs and SnNPs; for these NPs no MIC value could be determined for the tested strain, therefore concentrations of 1,000, 500, 250 and 125 µg/mL, respectively, were tested) were prepared in Brain Heart Infusion Broth (BHI; Merck, Darmstadt, Germany) with the addition of 2 % sucrose (Merck, Darmstadt, Germany).

Subsequently, the *in vitro* antibiofilm activity of the NPs were evaluated using the crystal violet binding assay modified according to the method described by Jardak et al. [23]. *P. aeruginosa* PAO1 strain was first incubated in 5 mL BHI medium at 37 °C for 24 h. The resulting culture was adjusted to approximately 1×10^6 CFU/mL with 2 % sucrose added to the BHI. Then 10 µL of this suspension was added to each well of the microtitre plate, followed by the addition of 140 µL of the modified medium with NPs at an appropriate concentration. The same procedure was used for the control groups, but no NPs were added. The plates were incubated at 37 °C for 24 h to allow biofilm formation. Biofilm formation was quantified using a crystal violet binding assay. Absorbance measurements were performed using a microplate reader (BioTek µQuant, BioTek Inc., Winooski, VT, USA) at a wavelength of 595 nm. The percentage of inhibition of biofilm formation was calculated using the formula given.

% inhibition of biofilm formation = $[(C - B) - (T - B)] / [(C - B)] \times 100$ (where C; OD values of the control samples, B; OD values of the blank samples, T; OD values of the test samples).

2.8 Anti- QS activity

Anti- QS activity was evaluated with the reporter strain *C. violaceum* ATCC 12472. The minimum inhibitory concentrations (MIC) of the NPs were determined before the test (the MIC could not be determined for SnNP only). The experimental protocol was based on the method described by Batohi et al. [24]. Cultures of *C. violaceum* ATCC 12472 were grown in Luria–Bertani (LB) broth (Merck, Darmstadt, Germany) alone for the control group and in LB broth with NPs at concentrations below the MIC for the experimental group. The cultures were incubated at 30 °C for 24 h. After incubation, 1 mL aliquots were taken from each culture and centrifuged at 10,000 × *g* for 5 min. The resulting bacterial pellets were resuspended in 1 mL dimethyl sulphoxide (DMSO, Sigma-Aldrich, USA). Violacein production and inhibition were determined by measuring the absorbance at 585 nm wavelength according to the following formula.

Violacein inhibition (%) = [(OD585 nm Control – OD585 nm Test) / (OD585 nm Control)] × 100.

2.9 Cell culture

HCT-116 and SW480 colon cancer cell lines, A549 and H1975 lung cancer cell lines, and A2780 and OVCAR3 ovarian cancer cell lines were grown in RPMI-1640 medium supplemented with 10 % heat-inactivated fetal bovine serum, 1 % L-glutamine, and 1 % penicillin/streptomycin in 75 cm^2 flasks at 37 °C in a humidified incubator containing 5 % CO_2. When the cells reached 80 % confluency, they were passaged by trypsinization.

2.10 Cell viability

Cell viability analysis was performed to evaluate the anticancer activity of the NPs (Ag, Ni, Co, Cu, Fe, Zn, Ce, Sn and Ti) [25]. For this purpose, equal numbers of cells were seeded into each well of 96-well plates (5,000 cells/well). The plates were incubated overnight at 37 °C in a humidified incubator with 5 % CO_2 to allow for cell attachment. The next day, stock solutions of NPs were prepared in DMSO at a concentration of 4 mg/mL. After incubation in an ultrasonic bath followed by vortexing, the stock solutions were further diluted in cell culture medium. NPs were applied to the cells at a final concentration of 3.39 µg/mL, and the cells were incubated for 72 h. After incubation, MTT (3-(4, 5-dimethylthiazol-2-yl)-2,5-diphenyltetrazolium bromide) solution (5 mg/mL) was added to the wells. Following a 4-h incubation at 37 °C, the resulting formazan crystals were dissolved using a solvent containing SDS-HCl and incubated overnight at 37 °C. Absorbance was measured at 550 nm the following day. Cells in the control group were considered 100 % viable. NPs that reduced cell viability less than 50 % at a concentration of 3.39 µg/mL were further tested in a concentration range of 3.39–0.211 µg/mL and IC_{50} values were calculated using the GraphPad Prism 9 software. Cells in the control group were not treated with NPs but received DMSO at the same final concentration as that used in the NP-treated groups.

2.11 Statistical analysis of biological activity

In cell culture experiments, statistical analysis was performed to determine the differences between the groups that were treated with or without NPs. Data are presented by mean ± standard deviation. One-way ANOVA or the Kruskal–Wallis test was used, a p-value of <0.05 was considered statistically significant. Multiple comparisons were performed using the One-Way ANOVA test and the Tukey test was used for post-hoc comparisons in antibiofilm and anti-QS detection experiments. Each experiment was performed in triplicate. Data are presented as means and standard deviations. All analyses were performed using GraphPad Prism software (version 9.0, Boston, MA, USA).

3 Results

3.1 Total phenolic content

The total phenolic content of the total extracts was determined by Folin–Ciocalteu method. Calibration curve was drawn using absorbance data of gallic acid against concentration. The regression equation was $y = 0.0291x + 0.0032$ and $R^2 = 0.9961$. Total phenolic content of total extracts was calculated as GAE. The results are described in Table 1.

Total phenolic content of each extract (TE1, TE2) was determined by the Folin–Ciocalteu method. Based on the obtained data, the extract (TE2) with the highest phenolic content was selected for the next stages of the study. The total extract (TE2) and separated into three sub-extracts as hexane sub-extract (HSE), ethyl acetate sub-extract (EASE) and aqueous sub-extract (ASE) by liquid–liquid extraction. The total phenolic content of each sub-extract was also determined by the Folin–Ciocalteu method. Calibration curve was drawn using absorbance data of gallic acid against concentration. The regression equation was $y = 12.001x + 0.0738$ and $R^2 = 0.9941$. Total phenolic content of total extracts was calculated as GAE. The results are described in Table 2.

3.2 Optimization and characterization

During the synthesis of NPs, the extract amount and incubation time were optimized using UV–vis spectroscopy. In extract optimization, 2, 3 and 4 mg extract amounts were tried except FeNPs. For FeNPs, 15, 20 and 25 mg extract amounts were tried. In incubation time optimization, 2, 3 and 4 h were tried. UV–vis region images obtained during optimization are shown in Figures S1 and S2. Optimized conditions and absorption peaks for each NPs are given in Table 3.

Optical microscope images of Ag, Ni, Co, Cu, Fe, Zn, Ce, Sn, Ti NPs synthesized with apple extract are shown in

Table 1: Total phenolic content of total extracts.

	mg GAE/g dry extract	
Extract Name	**Mean**	**SD**
TE1	18.1222078	0.85967999
TE2	32.367	2.23832434

Table 2: Total phenolic content of sub-extracts.

	mg gallic acid equivalent/g dry extract	
Extract Name	**Mean**	**SD**
HSE	13.8740	1.8329
EASE	39.3374	2.4371
ASE	20.2404	2.3802

Table 3: Optimized conditions and absorption peaks for the synthesis of NPs. Three different extract amounts and three different durations were tested for volume optimization. NPs with the highest absorption in UV–visible spectroscopy were selected.

NPs	Extract amount (mg)	Incubation time (h)	UV–vis peak
AgNPs	3	4	435 nm
NiNPs	4	3	240 nm
CoNPs	2	3	430 nm
CuNPs	4	4	295 nm
FeNPs	20	4	330 nm
ZnNPs	4	2	362 nm
CeNPs	4	3	305 nm
SnNPs	3	3	280 nm
TiNPs	3	2	250 nm

Figure S3a – 3p. The solution obtained by mixing these NPs with pure water is dropped onto the SiO_2/Si substrate, which has been previously cleaned and kept on a hot plate at 70 °C, with the help of a pipette and a homogeneously distributed surface was obtained. The characterization problems such as dispersion and shedding, especially in powder NPs samples, are thus solved.

Figure 1a–i present SEM images of Ag, Ni, Co, Cu, Fe, Zn, Ce, Sn and Ti NPs synthesized with apple extract at a magnitude of 5,000×. SEM measurements were made at high resolution under 20 KV.

Figure S4 shows the EDX analysis of Ag, Ni, Co, Cu, Fe, Zn, Ce, Sn, Ti NPs synthesized from apple extract on SiO_2/Si substrate that the weight percentages of Ag NPs are approximately 0.68 % Mg (magnesium), 99.32 % Ag (silver) while the atomic percentages of Ag NPs are approximately 2.97 % Mg (magnesium), 97.03 % Ag (silver). The weight percentages of Ni NPs are approximately 2.93 % C (carbon), 20.55 % O (oxygen), 1.10 % Si (silicon), 75.42 % Ni (nickel), while the atomic percentages of Ni NPs are approximately 8.55 % C (carbon), 45.04 % O (oxygen), 1.37 % Si (silicon), 45.04 % Ni (nickel). The weight percentages of Co NPs are approximately 2.28 % C (carbon), 20.60 % O (oxygen), 0.93 % Si (silicon), 0.18 % Cl (chlorine), 76.01 % Co (cobalt), while the atomic percentages of Co NPs are approximately 6.77 % C (carbon), 45.89 % O (oxygen), 1.18 % Si (silicon), 0.18 % Cl (chlorine), 45.98 % Co (cobalt). The weight percentages of Cu NPs are approximately 2.28 % C (carbon), 19.39 % O (oxygen), 1.32 % Si (silicon), 77.01 % Cu (copper), while the atomic percentages of Cu NPs are approximately 7.14 % C (carbon), 45.55 % O (oxygen), 1.76 % Si (silicon), 45.55 % Cu (copper). The weight percentages of Fe NPs are approximately 5.03 % C (carbon), 20.33 % O (oxygen), 2.30 % Na (sodium), 1.36 % Si (silicon), 70.98 % Fe (iron), while the atomic percentages of Fe NPs are approximately 13.46 % C (carbon), 40.88 % O (oxygen), 3.22 % Na (sodium), 1.56 % Si (silicon), 40.88 % Fe (iron). The weight percentages of Zn NPs are approximately 19.46 % O (oxygen), 80.34 % Zn (zinc), while the atomic percentages of Fe NPs are approximately Zn NPs are approximately 50.00 % O (oxygen), 50.00 % Zn (zinc). The weight percentages of Ce NPs are approximately 1.36 % C (carbon), 14.29 % O (oxygen), 0.95 % Si (silicon), 83.41 % Ce (cerium), while the atomic percentages of Ce NPs are approximately 6.92 % C (carbon), 54.61 % O (oxygen), 2.07 % Si (silicon), 36.41 % Ce (cerium). The weight percentages of Sn NPs are approximately 1.48 % C (carbon), 20.86 % O (oxygen), 0.16 % Cl (chlorine), 77.50 % Sn (tin), while the atomic percentages of Sn NPs are approximately 5.91 % C (carbon), 62.54 % O (oxygen), 0.22 % Cl (chlorine), 31.22 % Sn (tin). The weight percentages of TiNPs synthesized from apple waste extract are approximately as follows: 0.82 % C (carbon), 37.07 % O (oxygen), 2.54 Na (sodium), 0.67 Si (silicon), 2.54 % Cl (chlorine) 56.35 % Ti (titanium). The atomic percentages of titanium NPs synthesized from apple waste extract are approximately 1.82 % C (carbon), 61.49 % O (oxygen), 2.93 Na (sodium), 0.64 Si (silicon), 2.54 % Cl (chlorine) 31.22 % Ti (titanium).

Figure 2 illustrates the Raman spectra of Ag, Ni, Co, Cu, Fe, Zn, Ce, Sn, Ti NPs measured under 532 nm laser excitation. Raman peaks of Ag NPs are stated at about 233 cm^{-1} mode, 470 cm^{-1} mode, 627 cm^{-1} mode, 1,292 cm^{-1} mode, 1,364 cm^{-1} mode, 1,544 cm^{-1} mode in close agreement with previous studies [26]. Raman peaks of Ni NPs are stated at about 500 cm^{-1} mode, 738 cm^{-1} mode, 1,076 cm^{-1} mode, 1,425 cm^{-1} mode in close agreement with previous studies [27]. Raman peaks of Co NPs are stated at about 190 cm^{-1} mode, 429 cm^{-1} mode, 469 cm^{-1} mode, 511 cm^{-1} mode, 629 cm^{-1} mode, 685 cm^{-1} mode in close agreement with previous studies [28]. Raman peaks of Cu NPs are stated at about 286 cm^{-1} mode, 333 cm^{-1} mode, 520 cm^{-1} mode, 617 cm^{-1} mode, in close agreement with previous studies [29]. Raman peaks of Fe NPs are stated at about 219 cm^{-1} mode, 283 cm^{-1} mode, 397 cm^{-1} mode, 597 cm^{-1} mode, 671 cm^{-1} mode in close agreement with previous studies [30]. Raman peaks of Zn NPs are stated at about 307 cm^{-1} mode, 432 cm^{-1} mode, 494 cm^{-1} mode, 520 cm^{-1} mode, 603 cm^{-1} mode,

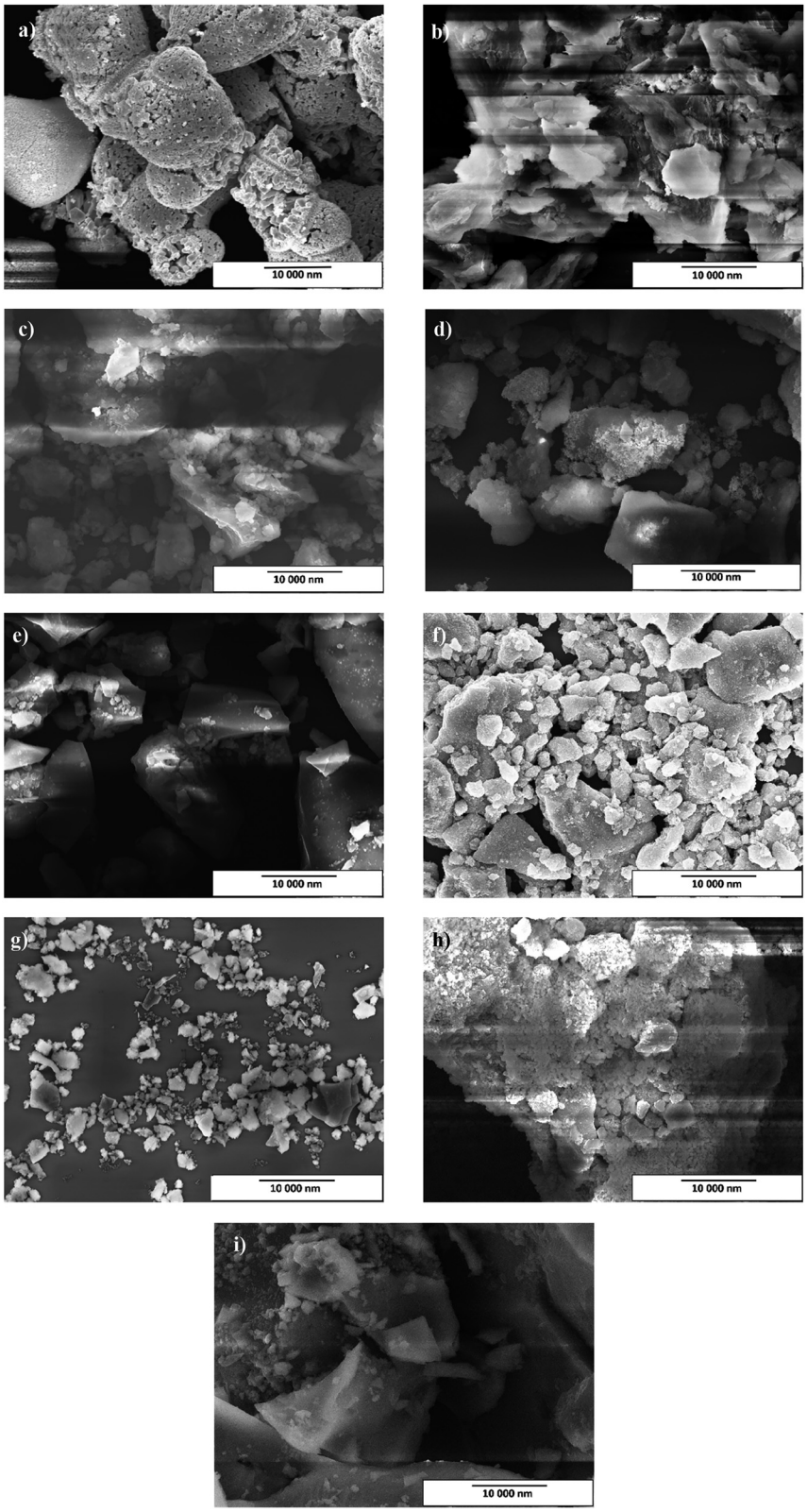

Figure 1: SEM images of various metal NPs synthesized from apple **extract** at 5,000× magnification: (a) AgNPs, (b) NiNPs, (c) CoNPs, (d) CuNPs, (e) FeNPs, (f) ZnNPs, (g) CeNPs, (h) SnNPs, (i) TiNPs.

707 cm^{-1} mode in close agreement with previous studies [31]. Raman peaks of Ce NPs are stated at about 465 cm^{-1} F_{2g} mode, 1,050 cm^{-1} weak band, in close agreement with previous studies [32]. Raman peaks of Sn NPs are stated at about 114 cm^{-1} mode, 131 cm^{-1} mode, 173 cm^{-1} mode, 224 cm^{-1} mode, 276 cm^{-1} mode, 330 cm^{-1} mode, 427 cm^{-1} mode, 458 cm^{-1} mode,

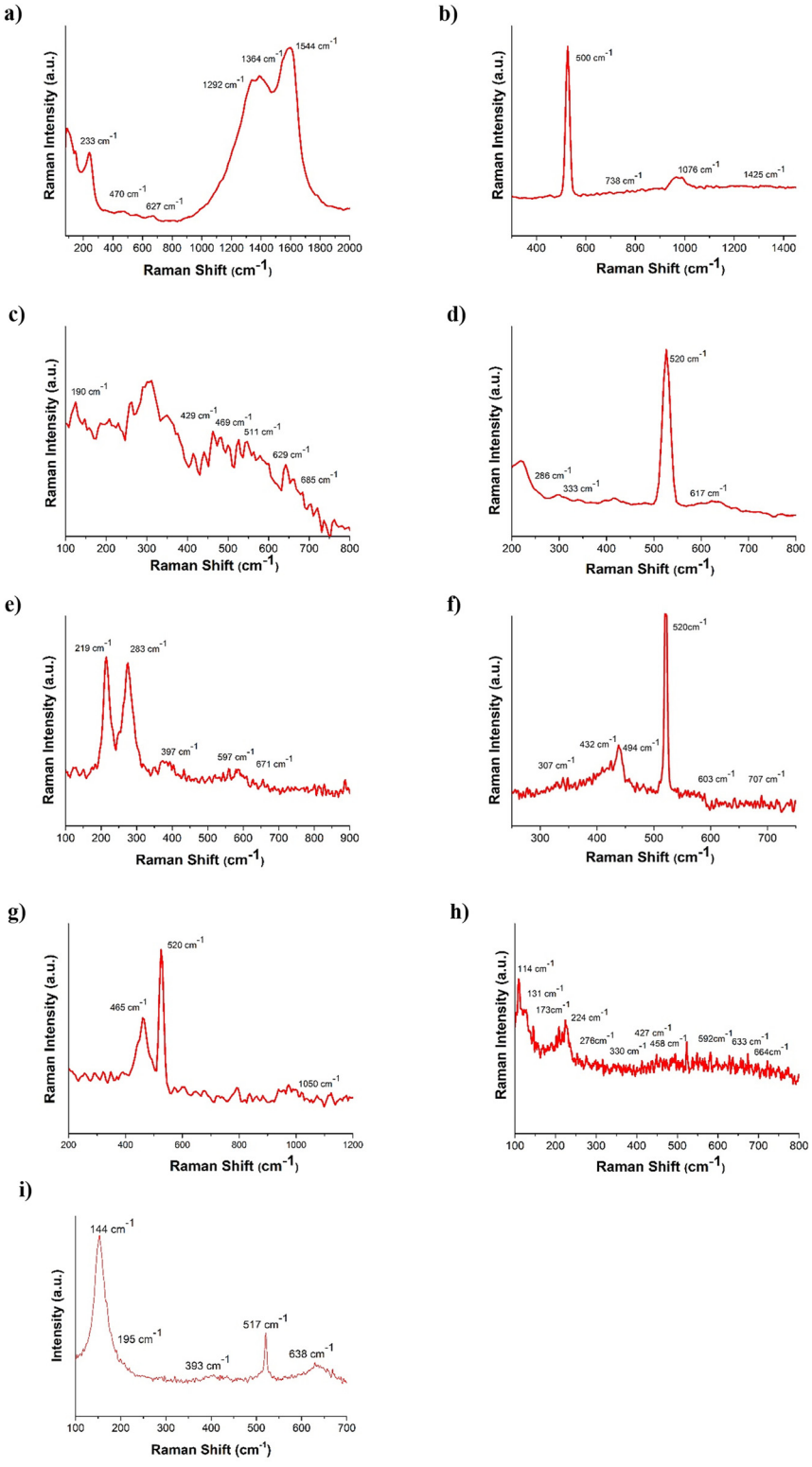

Figure 2: Raman spectra of a) AgNPs, b) NiNPs, c) CoNPs, d) CuNPs, e) FeNPs, f) ZnNPs, g) CeNPs, h) SnNPs and i) TiNPs synthesized from apple waste extract.

592 cm^{-1} mode, 633 cm^{-1} mode, 664 cm^{-1} mode in close agreement with previous studies [33]. Raman peaks of titanium NPs synthesized from apple waste extract are stated at about 144 cm^{-1} Eg mode, 195 cm^{-1} Eg mode, 393 cm^{-1} B1g mode, 517 cm^{-1} A1g mode, 638 cm^{-1} Eg mode in close agreement with previous studies [34].

AFM provides information about the shapes formed by Ag, Ni, Co, Cu, Fe, Zn, Ce, Sn NPs structures on the surface of

SiO_2/S substrate such as, 3D view of the NPs, amplitude measurements of NPs, surface topographies of the NPs and height profiles of the NPs (Figure S5). Ag NPs thickness measurements were approximately 120 nm, Ni NPs thickness measurements were approximately 60 nm, CoNPs thickness measurements were approximately 30 nm, Cu NPs thickness measurements were approximately 120 nm, Fe NPs thickness measurements were approximately 45 nm, ZnNPs thickness measurements were approximately 30 nm, CeNPs thickness measurements were approximately 50 nm, SnNPs thickness measurements were approximately 90 nm.

3.3 Antibacterial activity

AgNPs proved to be the most comprehensive and effective antibacterial agent and had the lowest MIC values against all strains tested. It demonstrated significant efficacy at minimal doses, namely 15.625–31.25 µg/mL, against bacteria such as *S. epidermidis* ATCC 12228 and *C. violaceum* ATCC 12472. CuNPs, similar to AgNPs, had antibacterial activity against most strains. The MIC values ranged from 15.625 to 1,000 µg/mL. The NPs showed significant activity against *S. epidermidis* strain ATCC 12228 at a concentration of 15.625 µg/mL. In addition, similar to AgNPs, these NPs were effective against both Gram-positive and Gram-negative bacteria. ZnNPs showed moderate antibacterial activity against bacterial species. The MIC values were predominantly in the range of 62.5–500 µg/mL. It is worth mentioning that these NPs showed activity especially in the strains of *P. aeruginosa* (ATCC 27853 and PAO1) tested at very high concentrations (2,000 µg/mL). Like AgNPs and CuNPs, these NPs also showed higher antibacterial activity against Gram-positive species such as *S. epidermidis* ATCC 12228, *S. aureus* ATCC 25923 and *B. subtilis* ATCC 6633. After NPs such as AgNPs, CuNPs and ZnNPs, CoNPs were the only NPs that showed antibacterial activity in the concentration range tested. CoNPs attracted attention with its MIC value of 125 µg/mL, especially with some strains such as *S. epidermidis* ATCC 12228 and *C. violaceum* ATCC 12472. NiNPs, CeNPs, SnNP, TiNPs generally showed high MIC values (≥1,000 µg/mL) and no microbial inhibition was observed in some strains tested with these NPs. It appears that the antibacterial effect of these NPs is limited and they should be used at higher concentrations. The lowest antibacterial activity was observed with SnNPs and TiNPs (Table 4).

3.4 Antibiofilm activity

This study shows the effects of different concentrations of NPs (sub-MIC; MIC/2, MIC/4, MIC/8 and MIC/16) on the biofilm formation of *P. aeruginosa* PAO1. The results for AgNPs showed that biofilm formation was strongly inhibited, especially at the MIC/2 and MIC/4 concentrations, and biofilm production was significantly reduced even at the MIC/16 concentration. It is clear that AgNPs can suppress biofilm formation even at concentrations below the MIC (Figure S6a). The effect of CuNPs concentrations on biofilm formation is shown in Figure S6b. The results show that CuNPs only cause a significant inhibition of biofilm formation at the MIC/2 concentration (22.39 %) and that this effect decreases significantly at other concentrations. Figure S6c shows the effects of different ZnNPs concentrations on biofilm formation. The results show that ZnNPs significantly inhibited biofilm formation at MIC/2 (56.39 %) and MIC/4 (55.09 %) concentrations, while this effect significantly decreased at lower concentrations (MIC/8 and MIC/16).

Table 4: Minimum inhibitory concentration values of metal NPs.

	MIC values of NPs (µg/mL)									
Test strains	**AgNPs**	**NiNPs**	**CeNPs**	**SnNPs**	**TiNPs**	**FeNPs**	**CoNPs**	**ZnNPs**	**CuNPs**	**Cip[a] (µg/mL)**
S. aureus ATCC 25923	31.25	1,000	2,000	2,000	–	–	500	62.5	250	0.5
S. aureus ATCC 43300	62.5	1,000	2,000	–	–	2,000	500	250	250	0.5
B. subtilis ATCC 6633	62.5	1,000	–	–	–	500	500	62.5	500	0.0625
S. epidermidis ATCC 12228	15.625	500	1,000	1,000	–	2,000	125	62.5	15.625	0.25
E. faecalis ATCC 29212	125	125	2,000	1,000	2,000	1,000	1,000	500	1,000	62.5
E. coli ATCC 25922	125	2,000	–	–	–	–	1,000	500	250	<0.25
P. aeruginosa ATCC 27853	125	–	–	–	–	2,000	1,000	2,000	500	<0.25
K. pneumoniae ATCC 13883	125	250	–	–	–	–	250	125	500	0.125
C. violaceum ATCC 12472	31.25	1,000	2,000	–	2,000	1,000	125	250	125	[b]
P. aeruginosa ATCC PA01	62.5	1,000	–	–	2,000	2,000	250	2,000	1,000	[b]

–, indicates that no MIC value was detectable in the tested concentration range. [a]Ciprofloxacin. [b]not performed for those strains.

Figure S6d analyzes the effects of different CoNPs concentrations (MIC/2, MIC/4, MIC/8 and MIC/16) on biofilm formation of the *P. aeruginosa* PAO1 strain. The results show that the highest biofilm inhibition occurred at the MIC/2 concentration (70.38 %), while the lowest inhibition occurred at MIC/16 (13.77 %). Figure S6e analyzes the effect of NiNPs on the biofilm formation of *P. aeruginosa* PAO1. While an inhibition of 72.03 % was observed at the MIC/2 concentration, this effect gradually decreased at lower concentrations, dropping to 2.94 % at MIC/16. When evaluating the potential effects of FeNPs on *P. aeruginosa* PAO1 biofilm formation, a limited inhibition of 21.13 % was observed at the highest concentration, MIC/2, and no inhibitory effect on the biofilm was observed at all other concentrations (MIC/4, MIC/8, MIC/16) (Figure S6f). In Figure S6g, 28.70 % inhibition of biofilm was observed at the highest concentration of 1,000 µg/mL for CeNPs, but this effect decreased significantly with decreasing concentrations. Another noteworthy point is that the MIC value for CeNPs could not be determined in advance. This indicates that CeNPs showed no bacteriostatic or bactericidal effect at the concentrations in the tested range and its ability to suppress biofilm formation was quite limited. At the three highest concentrations of SnNPs (1,000, 500 and 250 µg/mL), similar biofilm inhibition values of 60.99 %, 54.72 % and 53.10 % were observed, respectively. On the other hand, this effect decreased significantly at 125 µg/mL, dropping to 16.31 %. The minimum inhibitory concentration (MIC) value for SnNPs could not be determined. These results show that SnNPs have no bacteriostatic effect,but can significantly suppress biofilm formation at high concentrations (Figure S6h). For TiNPs, 38.04 % inhibition was achieved at the highest concentration (MIC/2), and this value decreased significantly at lower concentrations (Figure S6i).

In this study, the effects of different metal NPs (AgNPs, CuNPs, ZnNPs, CoNPs, NiNPs, FeNPs, CeNPs, SnNPs and TiNPs) at concentrations below the MIC (MIC/2, MIC/4, MIC/8, MIC/16) on the biofilm formation of *P. aeruginosa* PAO1 were comparatively investigated. The results showed that the inhibition of the biofilm varied greatly depending on the type of NPs and the concentration applied.

The NPs that showed the strongest antibiofilm activity was AgNPs, which achieved an inhibition of over 90 %, especially at the concentrations MIC/2 and MIC/4 and even showed a significant effect at MIC/16. ZnNPs, SnNPs and CoNPs also caused significant biofilm inhibition at high concentrations, but their activities decreased significantly at lower concentrations. Although SnNPs did not exhibit antibacterial activity, their efficacy in biofilm inhibition suggests that these particles likely influence the biofilm response independent of cell death.

3.5 Anti-QS activity

In this study, the inhibitory effect of different metal NPs on the production of violacein, an indicator of QS in strain *C. violaceum* ATCC 12472 was investigated. The results obtained show that the NPs exhibit significant differences in terms of their anti-QS potential. The highest inhibition rate was observed for CuNPs with 90.74 % at MIC/2 concentration. These NPs were followed by AgNPs (72.05 %), NiNPs (72.03 %) and ZnNPs (63.01 %). AgNPs in particular provided a remarkable profile by achieving a high level of inhibition with a very low MIC value of only 31.25 µg/mL. On the other hand, TiNPs (54.57 %), SnNPs (43.0 %) and CeNPs (30.59 %) showed moderate QS inhibition. The effect of NPs such as FeNPs (21.08 %) and CoNPs (13.51 %) were quite limited. SnNPs, whose MIC value could not be determined, only showed a significant effect at the highest concentration tested. NPs such as CeNPs, FeNPs and CoNPs can be considered as agents with low therapeutic potential in terms of QS suppression due to their high MIC values in addition to low inhibition rates (Figure S7).

Considering the results, CuNPs and AgNPs stand out as leading NPs with high capacity to inhibit QS and can be evaluated for potential applications. However, it should be emphasized that the anti-QS effects should be interpreted not only by the percentage of inhibition but also by the effect concentration.

3.6 Effects of NPs on HCT-116 colon cancer cell line

Ag, Co, Cu, Zn and Ni were effective at a single concentration of 3.39 µg/mL in HCT-116 cells. The results showed that although Ag, Co, and CuNPs did not reduce viability below 50 %, they still significantly decreased cell viability at this concentration ($p < 0.0001$), as did ZnNPs ($p < 0.01$). Since NiNPs reduced cell viability to below 50 % at 3.39 µg/mL, they were further tested across a concentration range of 0.211–3.39 µg/mL, and the IC_{50} value was calculated. NiNPs significantly decreased cell viability at both 3.39 µg/mL ($p < 0.001$) and 1.695 µg/mL ($p < 0.05$), with an IC_{50} value of 2.66 ± 0.33 µg/mL (Figure 3).

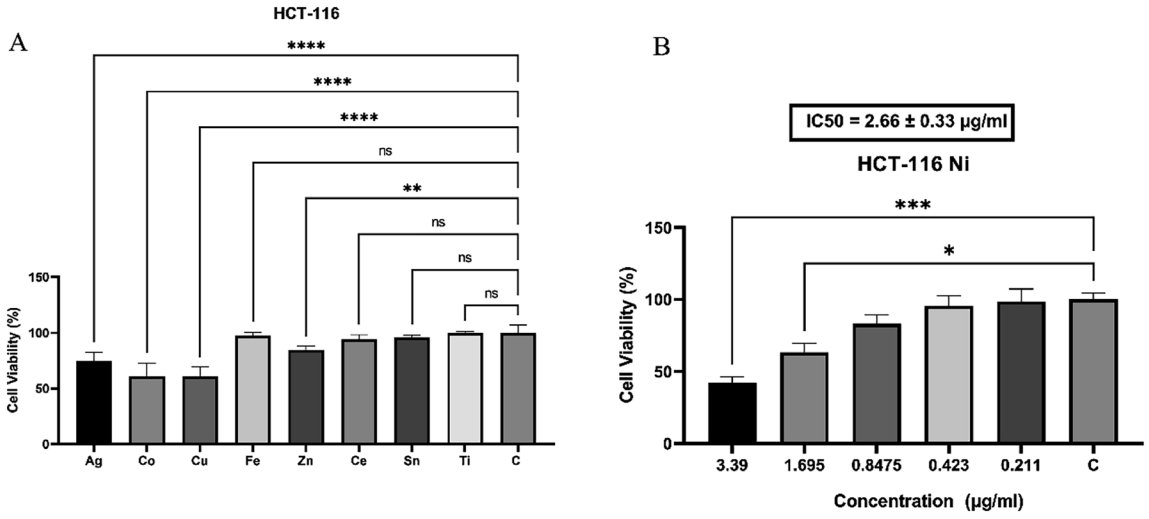

Figure 3: Effect of Ag, Co, Cu, Fe, Zn, Ce, Sn, Ti (3.39 µg/mL) and Ni NPs (0.211–3.39 µg/mL) on HCT-116 cell viability. (***$p < 0.001$; ****$p < 0.0001$; **$p < 0.01$, *$p < 0.05$ indicates statistically significance compared to the control group).

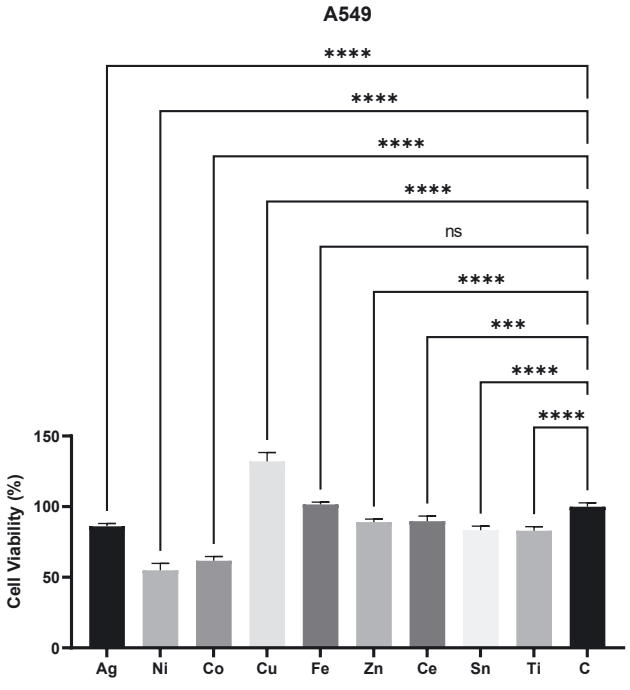

Figure 4: Effect of Ag, Ni, Co, Cu, Fe, Zn, Ce, Sn, Ti (3.39 µg/mL) on A549 cell viability (***$p < 0.001$; ****$p < 0.0001$ indicates statistically significance compared to the control group).

3.7 Effects of NPs on A549 lung cancer cell line

Ag, Ni, Co, Zn, Sn, and Ti NPs ($p < 0.0001$), as well as CeNPs ($p < 0.001$), significantly decreased the viability of A549 cells. Among them, NiNPs reduced cell viability to 54.88 ± 4.96 %, and CoNPs to 61.73 ± 2.93 %, making Ni and Co the most effective in reducing A549 cell viability. In contrast, CuNPs significantly increased A549 cell viability ($p < 0.0001$) (Figure 4).

3.8 Effects of NPs on A2780 ovarian cancer cell line

Among all NPs, Co, Zn, Ni, and Cu significantly reduced cell viability at a concentration of 3.39 µg/mL. Co and ZnNPs decreased cell viability to 59.40 ± 2.33 % and 87.39 ± 4.95 %, respectively ($p < 0.0001$ and $p < 0.05$). Since NiNPs and CuNPs reduced cell viability below 50 %, they were further tested across a concentration range of 0.211–3.39 µg/mL, and IC_{50} values were calculated. The IC_{50} value for NiNPs were 1.29 ± 0.62 µg/mL, while the IC_{50} value for CuNPs was 0.797 ± 0.062 µg/mL, making Cu the most effective NPs against A2780 cell line. NiNPs and CuNPs significantly decreased A2780 cell viability within the concentration ranges of 0.211–3.39 µg/mL and 0.8475–3.39 µg/mL, respectively (Figure 5).

3.9 Effects of NPs on H1975 lung cancer cell line

Among all tested NPs, NiNPs and CoNPs decreased H1975 cell viability to 50.08 ± 6.355 % and 62.49 ± 4.815 %, respectively; while opposite viability enhancing effects were determined for FeNPs (Figure 6).

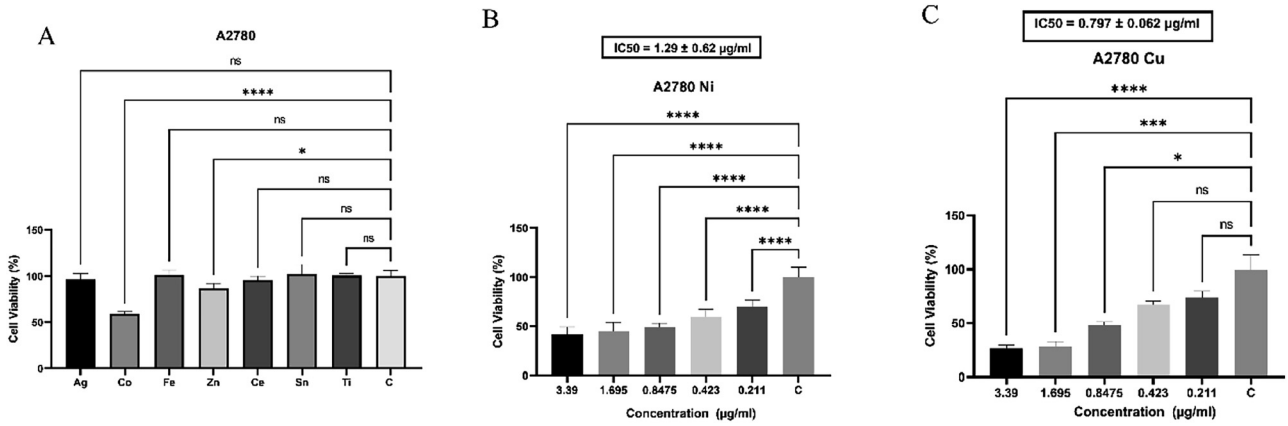

Figure 5: Effect of Ag, Co, Fe, Zn, Ce, Sn, Ti (3.39 µg/mL), NiNPs and CuNPs (0.211–3.39 µg/mL) on A2780 cell viability (A) effect of NiNPs (B) and CuNPs (C) (*p < 0.05; **p < 0.01;***p < 0.001; ****p < 0.0001 indicates statistically significance compared to the control group).

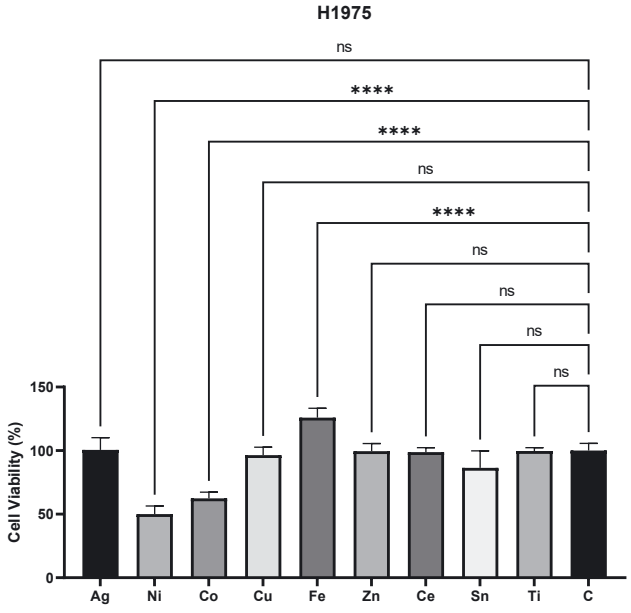

Figure 6: Effect of Ag, Ni, Co, Cu, Fe, Zn, Ce, Sn, Ti (3.39 µg/mL) on H1975 cell viability. (****p < 0.0001 indicates statistical significance compared to the control group).

3.10 Effects of NPs on OVCAR-3 ovarian cancer cell line

Among all tested NPs: CeNPs, SnNPs, TiNPs, NiNPs, CoNPs, and CuNPs significantly reduced cell viability at a single concentration of 3.39 µg/mL on OVCAR-3 cells. The results showed that although CeNPs, SnNPs, and TiNPs did not reduce viability below 50 %, they still significantly decreased cell viability at this concentration (Figure 7a). On the other hand, more effective NiNPs, CoNPs, and CuNPs, which reduced cell viability below 50 % at 3.39 µg/mL, were further tested across a wider concentration range. The IC_{50} values for NiNPs, CoNPs, and CuNPs were determined to be 1.633 ± 0.245 µg/mL (Figure 7b), 2.082 ± 0.23 µg/mL (Figure 7c), and 2.346 ± 0.598 µg/mL (Figure 7d), respectively.

3.11 Effects of NPs on SW480 colon cancer cell line

Among the tested NPs, Ni was identified as the most effective, reducing SW480 colon cancer cell viability to 57.16 ± 3.20 % (p < 0.0001), while the viability values for the other effective NPs, Co, Cu and Zn was 65.47 ± 2.14 % (p < 0.0001), 75.77 ± 3.27 % (p < 0.0001) and 91.79 ± 7.58 (p < 0.05) respectively. In contrast, FeNPs were found to increase cell viability (p < 0.0001) (Figure 8).

4 Discussion

The physical and chemical properties of NPs can be significantly altered depending on the synthesis method and plant source used. This variability affects properties such as particle size, morphology, surface charge, stability, and surface functional groups, thus determining their potential applications in analytical, biomedical, and industrial applications. In this study, the highest phenolic content of different extracts prepared from industrial apple waste was determined. Ethanol extract metal NPs with the highest phenolic content were synthesized. When the characterization studies were examined, it was seen that a successful synthesis was achieved. UV–vis region spectra are compatible with the literature. Raman spectrum shows the presence of functional groups that increase stability on the surface of the

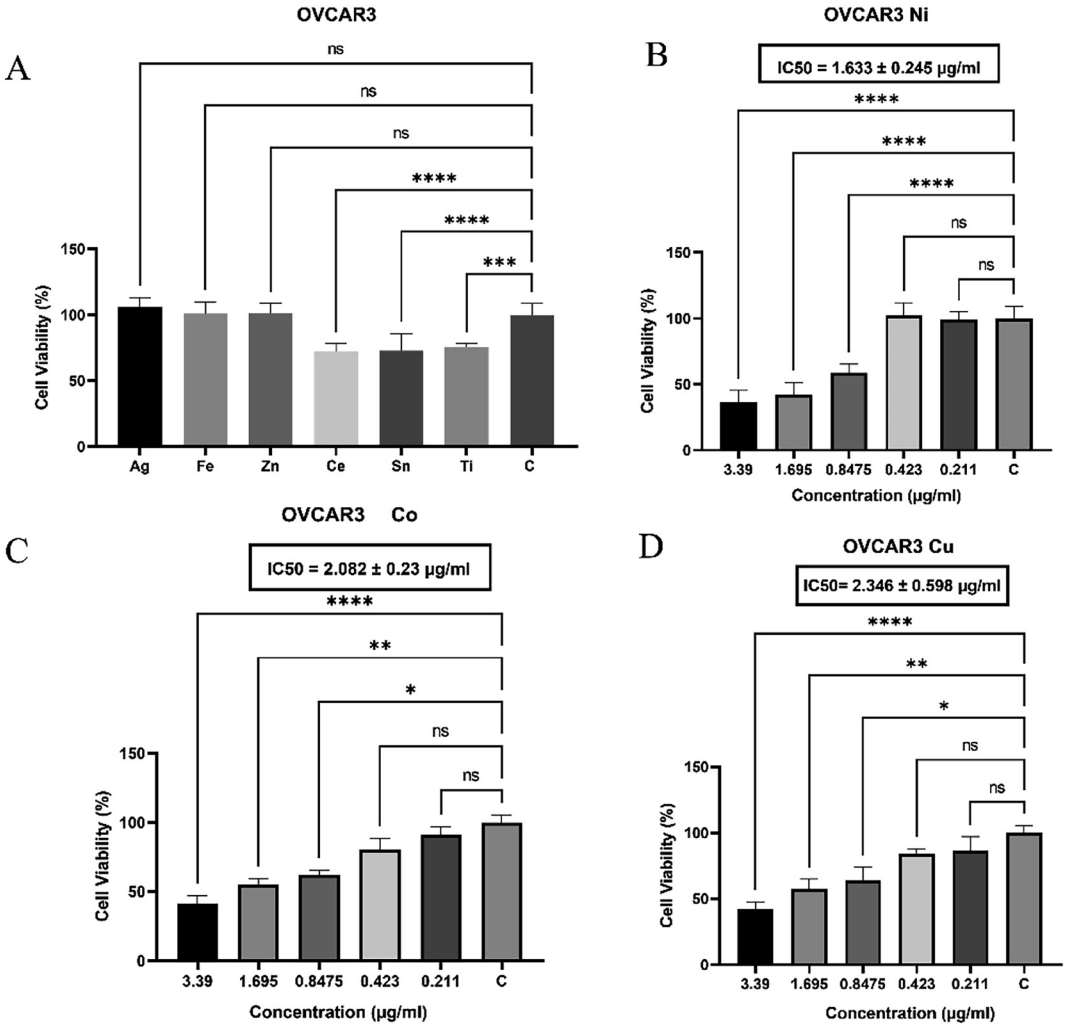

Figure 7: Effect of Ag, Fe, Zn, Ce, Sn, Ti (3.39 µg/ml) on OVCAR cell viability (a). (*p < 0.05; **p < 0.01; ***p < 0.001; ****p < 0.0001 indicates statistical significance compared to the control group.) Effect of Ni (b), Co (c) and Cu (d) NPs on OVCAR-3 cell viability.

NPs. When EDX results were examined, it was confirmed that the synthesized NPs were free from impurities. SEM images reveal that the size of the NPs is smaller than 100 nm. All characterization findings obtained show that the structural and optical properties of the NPs prepared by the green synthesis method are consistent with the studies reported in the literature, proving that this method offers a reliable and effective alternative synthesis approach.

In this work, nine metal NPs prepared from apple pulp (AgNPs CuNPs, ZnNPs, CoNPs, NiNPs, FeNPs, CeNPs, SnNPs, TiNPs) were analysed for their antibacterial, antibiofilm and anti- QS properties. The results showed a clear hierarchy of efficacy: AgNPs and CuNPs were the most effective broad-spectrum agents, while ZnNPs and CoNPs showed moderate activity and NiNPs, FeNPs, CeNPs and TiNPs showed relatively weak or no effect. It is known that silver NPs have strong antibacterial and antibiofilm properties that often outperform other metal-based NPs [35]. In this study, the antibacterial activity of CuNPs, another NPs that showed broad antibacterial activity, is controversially discussed in the literature. In the study by Elshaer and Shaaban [36], they found that CuNPs showed no antibacterial activity in some strains of *rA. baumannii*, *K. pneumoniae* and *P. aeruginosa* (strain PAO1) and suggested that this phenomenon could be related to the fact that CuNPs are cofactor of enzymes such as cytochrome c oxidase and NADH dehydrogenase, as these are important for cell growth. Certain metal NPs such as FeNPs and CeNPs also showed relatively high antibacterial activity in this study. These results are also consistent with the study by Masadeh et al. [37]. Masadeh et al. (2015) found that CeNPs and FeNPs only insufficiently inhibit microbial growth [38]. The observed moderate antibacterial effect of ZnNPs, CoNPs and NiNPs correlates with previous research results indicating that these NPs can inhibit microbial

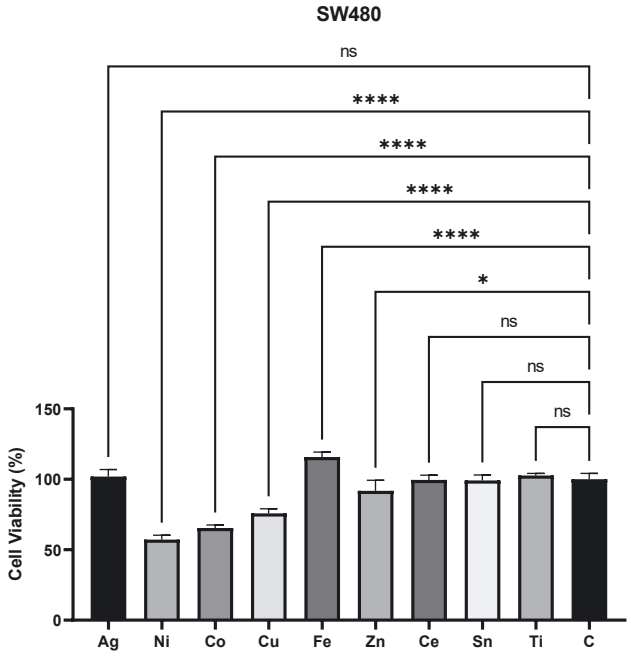

Figure 8: Effect of Ag, Ni, Co, Cu, Fe, Zn, Ce, Sn, Ti (3.39 µg/mL) on SW480 cell viability (*$p < 0.05$, ****$p < 0.0001$ indicates statistically significance compared to the control group).

growth and biofilm formation, but often at higher concentrations than AgNPs or CuNPs. The observed moderate antibacterial effect of ZnNPs, CoNPs and NiNPs correlates with previous research results indicating that these NPs can inhibit microbial growth and biofilm formation, but often at higher concentrations than AgNPs or CuNPs [39]. Silver NPs in particular have shown significant antiviral properties in previous research. Aflakian and Hashemitabar [40] reported that green-synthesised AgNPs at subinhibitory concentrations inhibited biofilm formation of *P. aeruginosa* PAO1 by about 78 % and showed dose-dependent suppression of various virulence factors regulated by QS, including LasB elastase, LasA protease, pyocyanin and motility. The ability of AgNPs to reduce biofilm development and bacterial pathogenicity at sublethal concentrations is a significant advantage as they effectively neutralise the pathogen. Copper NPs also exhibit high bioactivity. A recent study showed that biosynthesised CuNPs not only reduced bacterial adhesion but also eradicated mature biofilms of various Gram-negative pathogens, including *A. baumannii*, *K. pneumoniae* and *P. aeruginosa* [36].

An intriguing finding of our results was that SnNPs showed a remarkable antibiofilm effect, although it had no measurable antibacterial activity. In other words, SnNPs were able to prevent the formation of biofilms without killing the free-living bacteria. This pattern suggests that SnNPs may specifically interfere with biofilm formation pathways (e.g. surface adhesion or cell-cell signalling) rather than exerting direct toxic effects on bacterial growth. Similar observations have also been made with other systems. For example, it has been shown that antimony-doped tin oxide NPs significantly inhibit biofilm formation by both uropathogenic *E. coli* and *S. aureus* [41]. The ATO NPs (antimony tin oxide) in this work reduced critical virulence factors of biofilms (e.g. reduced cell surface hydrophobicity and hemolytic activity) and downregulated a biofilm-associated gene (*hla*, encoding α-hemolysin in *S. aureus*) without having a significant bactericidal effect.

The different functions of the metal NPs can be explained by their unique mechanisms of action. AgNPs and CuNPs show a comprehensive efficacy that can be attributed to various simultaneous processes at the cellular level. Silver NPs emit Ag^+ ions that bind strongly to bacterial proteins, enzymes and DNA, thereby disrupting important processes. They also produce reactive oxygen species (ROS) and trigger oxidative stress in the cell. Due to their small size and high surface reactivity, they can potentially cause direct damage to cell membranes [42]. Copper NPs exhibit several of these mechanisms: Cu^{2+} ions released from CuNPs can generate hydroxyl radicals that lead to oxidative damage. Copper ions and NPs destabilise bacterial membranes and proteins. In a recently developed design with quercetin-loaded CuNPs, the copper component showed the ability to destroy bacteria by disrupting the integrity of the cell membrane [43].

NiNPs and CoNPs appear to act in a similar way, albeit with less efficacy. Their antibacterial effect is associated with the disruption of membranes, denaturation of proteins and impairment of DNA replication [44]. Zinc NPs, which are probably the form of ZnNPs used in our synthesis, function primarily through the generation of reactive oxygen species (ROS) and the release of Zn^{2+} ions. Oxidative stress caused by ZnNPs has the potential to damage bacterial membranes and intracellular components. In addition, Zn^{2+} can bind to proteins and nucleic acids, leading to disruption of metabolic processes. In particular, sublethal ZnNPs can modulate bacterial signalling, e.g. by downregulating the expression of QS genes [45].

In this study, numerous NPs were tested for QS activity at non-lethal concentrations below the MIC range, suggesting that their antibiofilm effect is primarily due to antivirulence rather than direct bactericidal activity. Our results with AgNPs and CuNPs showed significant anti-QS activity, which is consistent with previous reports that certain metal NPs can serve as effective quorum quenchers. Zinc NPs have shown a significant reduction in the production of QS-driven virulence factors, including rhamnolipids, pyocyanin, pyoverdins and proteases, in *P. aeruginosa*. This effect is accompanied by a remarkable down-regulation of the

QS-regulating genes *lasI*, *lasR*, *rhlI*, *rhlR*, *pqsA* and *pqsR* [45]. Silver NPs have also been reported to disrupt QS circuits. In *P. aeruginosa*, green-synthesised AgNPs in subinhibitory doses not only reduced biofilm biomass but also suppressed the expression of QS-controlled biofilm genes [40]. Although the synthesized NPs showed promising antibacterial, antibiofilm, and anti- QS activities, this study has several limitations. The experiments were conducted *in vitro* under controlled laboratory conditions, which may not fully represent the complexity of biological environments. In addition, only a limited number of bacterial strains and signaling pathways were examined, and the molecular mechanisms underlying the observed effects were not explored in detail. Future studies involving a broader range of clinically relevant pathogens, gene expression analyses, and *in vivo* validation are needed to better understand the therapeutic potential and practical applicability of these NPs.

They are important to investigate the potential impact of the green synthesis method using apple pulp on the efficacy of the NPs. They are known that biogenic synthesis routes leave a coating of phytochemicals on the NPs that may affect their interactions with microorganisms. The flesh of apples contains an abundance of polyphenols, sugars and various organic acids, which probably act as reducing and stabilising agents for our metal salts. The biomolecules that coat the surface of the NPs can improve stability and biocompatibility and could also play a role in antibacterial activity. Plant capping agents have been shown to provide NPs with additional antibiofilm properties, for example by disrupting bacterial adhesion or QS signalling [46]. Many phytochemicals are known as QS inhibitors. Quercetin, a flavonoid found in fruits, is one such compound with anti-QS activity [38]. Although we have not specifically analysed the cap compounds on our apple pulp NPs, they are reasonable to assume that similar synergistic interactions may have occurred.

NiNPs were found to be the most effective in colon cancer cell lines, showing a greater cell viability-reducing effect in HCT-116 cells compared to SW480 cells. In A549 and H1975 lung cancer cell lines, as well as in the OVCAR-3 ovarian cancer cell line, NiNPs also demonstrated the highest efficacy among all NPs tested. The IC_{50} values of NiNPs were 2.66 ± 0.33 µg/mL for HCT-116, 1.29 ± 0.62 µg/mL for A2780, and 1.633 ± 0.245 µg/mL for OVCAR-3 cells. Although NiNPs did not reduce cell viability below 50 % in SW480, A549, and H1975 cells, they still significantly decreased viability in these lines. Notably, NiNPs exhibited the greatest activity against A2780 ovarian cancer cells across all tested cell lines. However, in the A2780 ovarian cancer cell line, CuNPs were the most effective, with an IC_{50} value of 0.797 ± 0.062 µg/mL – representing the highest level of inhibition observed for any NPs. CuNPs also reduced cell viability in HCT-116, SW480, and OVCAR-3 cells.

Among the tested cell lines, CoNPs exhibited their highest activity in the OVCAR-3 cell line.

This study has several limitations. First, the proportions of phytochemical components contained in the extracts obtained from apple waste on the NPs surface and how they contribute to biological activity have not been determined in detail. Furthermore, the mechanisms underlying the observed antibacterial, antibiofilm, and anti- QS effects, such as reactive oxygen species (ROS) production or changes in gene expression, have not been confirmed at the biochemical level. The biological tests used in this study were conducted on a limited number of bacterial and cancer cell lines; further tests with different strains may provide more comprehensive results. All biological assessments were conducted *in vitro*; therefore, the biocompatibility, toxicity, and efficacy of the NPs *in vivo* have not yet been established. Finally, the long-term stability, storage durability, and environmental impacts of the synthesized NPs have not been evaluated.

5 Conclusions

This study comprehensively demonstrates that industrial-scale apple waste can be used as an effective, environmentally friendly, and renewable biological resource in the green synthesis of various metal NPs. This approach, consistent with circular economy principles, enables both the transformation of industrial waste into high value-added nanomaterials and the reduction of the environmental burden associated with the use of chemical reducing agents. Optical and surface characterization analyses (UV–vis, Raman spectroscopy, AFM, EDX, and SEM) confirmed that the synthesized NPs were pure, stable, below 100 nm in size, and consistent with the structural and optical characteristics previously reported in the literature. Antimicrobial assessments revealed that AgNPs and CuNPs exhibited the most pronounced antibacterial, antibiofilm, and anti-QS effects, whereas ZnNPs, CoNPs, and NiNPs showed more limited yet measurable inhibition. Notably, AgNPs demonstrated the strongest antimicrobial activity across all tested microorganisms, providing marked growth inhibition at concentrations of 15.625–31.25 µg/mL against *S. epidermidis* ATCC 12228 and *C. violaceum* ATCC 12472. In addition to suppressing bacterial proliferation, AgNPs significantly reduced biofilm formation even at low concentrations. CuNPs displayed a broad activity range between 15,625 and 1,000 µg/mL, while ZnNPs exhibited moderate antimicrobial

potential within the 62.5–500 µg/mL range. Although CoNPs and NiNPs achieved high biofilm inhibition at MIC/2 (70.38 % and 72.03 %, respectively), their activity declined substantially at lower concentrations. Although the MIC of SnNPs could not be established, they showed pronounced antibiofilm effects at 1,000–250 µg/mL. Interestingly, SnNPs inhibited biofilm formation and QS processes without displaying significant antibacterial activity, suggesting a selective mechanism targeting QS-mediated pathways. Cytotoxicity assays demonstrated that NiNPs possessed strong anticancer potential in HCT-116 ($IC_{50:}$ 2.66 ± 0.33 µg/mL), A2780 (IC_{50}: 1.29 ± 0.62 µg/mL), and OVCAR-3 (IC_{50}: 1.633 ± 0.245 µg/mL) cell lines. Among all tested NPs, the highest inhibition in the A2780 cell line was observed for CuNPs, with an IC_{50} value of 0.797 ± 0.062 µg/mL. Furthermore, CuNPs also displayed the strongest anticancer effect in the OVCAR-3 cell line. Taken together, these findings highlight NiNPs and CuNPs as particularly promising candidates for biomedical applications due to their potent anticancer properties.

Overall, the results demonstrate that apple waste offers an environmentally friendly, cost-efficient, and circular economy compatible platform for biogenic NPs synthesis, enabling the production of multifunctional nanomaterials with notable antimicrobial and anticancer activities. Nevertheless, to ensure the clinical or industrial feasibility of these NPs, further studies are required to elucidate their mechanisms of action, clarify the influence of phytochemical capping agents on biological performance, and comprehensively evaluate long-term stability, toxicity, and *in vivo* efficacy. Future studies evaluating the scalability and economic feasibility of this green synthesis approach, examining its adaptability to different types of industrial and agricultural waste, and investigating the effectiveness of the resulting NPs in targeted biomedical and antimicrobial applications will make significant contributions to the field of sustainable nanotechnology.

Acknowledgments: This study was financially supported by Ankara University BAP Research and Support Program under grant number TSA-2023-2753. Nuran GOKDERE thanks the financial support from the Scientific and Technological Research Council of Türkiye (TUBITAK) under the BIDEB/2211-A Ph.D. Batuhan OZTURK thanks the financial support from the Scientific and Technological Research Council of Türkiye (TUBITAK) under the BIDEB/2210-A MSc.

Author contributions: All authors have accepted responsibility for the entire content of this manuscript and approved its submission.

Conflict of interest: The authors state no conflict of interest.

Data availability statement: The datasets generated and/or analysed during the current study are available from the corresponding author on reasonable request.

References

1. Cendrowski A, Jakubowska Z, Przybył JL. Apple tree leaves (Malus domestica Borkh) as a valuable source of polyphenolic compounds with a high antioxidant capacity. Appl Sci 2024;14:3252.
2. Pascoalino LA, Finimundy TC, Pires TC, Pereira C, Barros L, Ferreira IC, et al. Investigating bioactive compounds in apple pomace: potential to develop high added-value products from an industrial surplus. Food Biosci 2025;63:105664.
3. Ramadan MF, Farag MA, editors. Mediterranean fruits bio-wastes: Chemistry, functionality and technological applications. Cham: Springer; 2022.
4. Liu H, Kumar V, Jia L, Sarsaiya S, Kumar D, Juneja A, et al. Biopolymer poly-hydroxyalkanoates (PHA) production from apple industrial waste residues: a review. Chemosphere 2021;284:131427.
5. Manrich A. Apple industry: wastes and possibilities. Int J Agric Res Environ Sci 2024;5:1–10.
6. Zaky AA, Witrowa-Rajchert D, Nowacka M. Turning apple pomace into value: sustainable recycling in food production–A narrative review. Sustainability 2024;16:7001.
7. Vandorou M, Plakidis C, Tsompanidou IM, Adamantidi T, Panagopoulou EA, Tsoupras A. A review on apple pomace bioactives for natural functional food and cosmetic products with therapeutic health-promoting properties. Int J Mol Sci 2024;25:10856.
8. Gullón P, Gullón B, Romaní A, Rocchetti G, Lorenzo JM. Smart advanced solvents for bioactive compounds recovery from agri-food by-products: a review. Trends Food Sci Technol 2020;101:182–97.
9. Aswathi VP, Meera S, Maria CA, Nidhin M. Green synthesis of nanoparticles from biodegradable waste extracts and their applications: a critical review. Nanotechnol Environ Eng 2023;8:377–97.
10. Abdel-Shafy HI, Mansour MS. Green synthesis of metallic nanoparticles from natural resources and food waste and their environmental application. In: Green metal nanoparticles: Synthesis, characterization and their applications. Beverly, Massachusetts, United States: Scrivener Publishing; 2018:321–85 pp.
11. Yadi M, Mostafavi E, Saleh B, Davaran S, Aliyeva I, Khalilov R, et al. Current developments in green synthesis of metallic nanoparticles using plant extracts: a review. Artif Cells Nanomed Biotechnol 2018;46:336–43.
12. Saratale RG, Saratale GD, Shin HS, Jacob JM, Pugazhendhi A, Bhaisare M, et al. New insights on the green synthesis of metallic nanoparticles using plant and waste biomaterials: current knowledge, their agricultural and environmental applications. Environ Sci Pollut Res 2018;25:10164–83.
13. Gökdere N, Rizvanoğlu SS, Emir E, Bostanci HE, Eryilmaz M, Atakol O, et al. Green synthesis and characterization of silver and zinc nanoparticles using Pyracantha coccinea M. Roem and their biological activities. Appl Organomet Chem 2025;39:e70391.
14. Islam MA, Islam M, Hasan R, Hossain MI, Nabi A, Rahman M, et al. Environmental spread of New Delhi metallo-β-lactamase-1-producing

multidrug-resistant bacteria in Dhaka, Bangladesh. Appl Environ Microbiol 2017;83:e00793-17.
15. World Health Organization. Global action plan on antimicrobial resistance. Geneva: World Health Organization; 2017. Available from: https://www.who.int/publications/i/item/9789241509763.
16. Uroz S, Dessaux Y, Oger P. Quorum sensing and quorum quenching: the yin and yang of bacterial communication. Chembiochem 2009;10: 205–16.
17. Nithya C, Begum MF, Pandian SK. Marine bacterial isolates inhibit biofilm formation and disrupt mature biofilms of Pseudomonas aeruginosa PAO1. Appl Microbiol Biotechnol 2010;88:341–58.
18. Rajeshkumar S. Anticancer activity of eco-friendly gold nanoparticles against lung and liver cancer cells. J Genet Eng Biotechnol 2016;14: 195–202.
19. Singh P, Pandit S, Mokkapati VRSS, Garg A, Ravikumar V, Mijakovic I. Gold nanoparticles in diagnostics and therapeutics for human cancer. Int J Mol Sci 2018;19:1979.
20. Ali MRK, Wu Y, Ghosh D, Do BH, Chen K, Dawson MR, et al. Correction to nuclear membrane-targeted gold nanoparticles inhibit cancer cell migration and invasion. ACS Nano 2020;14:12260.
21. Ainsworth EA, Gillespie KM. Estimation of total phenolic content and other oxidation substrates in plant tissues using Folin-Ciocalteu reagent. Nat Protoc 2007;2:875–7.
22. CLSI. Methods for dilution antimicrobial susceptibility tests for bacteria that grow aerobically; approved standard M07, 11th ed. Wayne (PA): Clinical and Laboratory Standards Institute; 2018. Available from: https://clsi.org/standards/products/microbiology/documents/m07/.
23. Jardak M, Mnif S, Ayed RB, Rezgui F, Aifa S. Chemical composition, antibiofilm activities of Tunisian spices essential oils and combinatorial effect against Staphylococcus epidermidis biofilm. LWT 2021;140:110691.
24. Batohi N, Lone SA, Marimani M, Wani MY, Al-Bogami AS, Ahmad A. Citral and its derivatives inhibit quorum sensing and biofilm formation in Chromobacterium violaceum. Arch Microbiol 2021;203:1451–9.
25. Mosmann T. Rapid colorimetric assay for cellular growth and survival: application to proliferation and cytotoxicity assays. J Immunol Methods 1983;65:55–63.
26. Joshi N, Jain N, Pathak A, Singh J, Prasad R, Upadhyaya CP. Biosynthesis of silver nanoparticles using Carissa carandas berries and its potential antibacterial activities. J Sol Gel Sci Technol 2018;86:682–9.
27. Rincón-Granados KL, Vázquez-Olmos AR, Rodríguez-Hernández AP, Vega-Jiménez A, Ruiz F, Garibay-Febles V, et al. Facile solid-state synthesis and in vitro study of the antibacterial activity of NiO and $NiFe_2O_4$ nanoparticles. Materialia 2021;15:100955.
28. El-Shafie AS, Ahsan I, Radhwani M, Al-Khangi MA, El-Azazy M. Synthesis and application of cobalt oxide (Co_3O_4)-impregnated olive stones biochar for the removal of rifampicin and tigecycline: multivariate controlled performance. Nanomaterials 2022;12:379.
29. Murthy PS, Venugopalan VP, Arunya DD, Dhara S, Pandiyan R, Tyagi AK. Antibiofilm activity of nano sized CuO. In: International conference on nanoscience, engineering and technology (ICONSET 2011). Chennai, India: IEEE; 2011:580–3 pp.
30. Chourpa I, Douziech-Eyrolles L, Ngaboni-Okassa L, Fouquenet JF, Cohen-Jonathan S, Soucé M, et al. Molecular composition of iron oxide nanoparticles, precursors for magnetic drug targeting, as characterized by confocal Raman microspectroscopy. Analyst 2005; 130:1395–403.
31. Pandey P, Parra MR, Haque FZ, Kurchania R. Effects of annealing temperature optimization on the efficiency of ZnO nanoparticles photoanode based dye sensitized solar cells. J Mater Sci Mater Electron 2017;28:1537–45.
32. Wang YJ, Dong H, Lyu GM, Zhang HY, Ke J, Kang LQ, et al. Engineering the defect state and reducibility of ceria based nanoparticles for improved anti-oxidation performance. Nanoscale 2015;7:13981–90.
33. Akyil C, Akdas G, Afsin P, Ürgen M. Freestanding SnO_2 films produced with anodic polarization in acidic media containing colloidal tin hydroxides. Mater Chem Phys 2019;221:263–71.
34. Chen M, Fan Q, Yu P, Chen K, Li P, Liang K. Engineering Ti_3C_2-MXene surface composition for excellent Li^+ storage performance. Molecules 2024;29:1731.
35. Jamkhande PG, Ghule NW, Bamer AH, Kalaskar MG. Metal nanoparticles synthesis: an overview on methods of preparation, advantages and disadvantages, and applications. J Drug Deliv Sci Technol 2019;53:101174.
36. Elshaer S, Shaaban MI. Antibiofilm activity of biosynthesized silver and copper nanoparticles using *Streptomyces* S29. AMB Express 2023;13: 139.
37. Masadeh MM, Karasneh GA, Al-Akhras MA, Albiss BA, Aljarah KM, Al-Azzam SI, et al. Cerium oxide and iron oxide nanoparticles abolish the antibacterial activity of ciprofloxacin against gram positive and gram negative biofilm bacteria. Cytotechnology 2015;67:427–35.
38. Serov DA, Gritsaeva AV, Yanbaev FM, Simakin AV, Gudkov SV. Review of antimicrobial properties of titanium dioxide nanoparticles. Int J Mol Sci 2024;25:10519.
39. Balogun SA, Abolarinwa TO, Adesanya FA, Ateba CN, Fayemi OE. Spectroscopic and antibacterial activities of cobalt and nickel nanoparticles: a comparative analysis. J Anal Sci Technol 2024;15:33.
40. Aflakian F, Hashemitabar G. Biosynthesized silver nanoparticles at subinhibitory concentrations as inhibitors of quorum sensing, pathogenicity, and biofilm formation in *Pseudomonas aeruginosa* PAO1. Heliyon 2025;11:e15200.
41. Park I, Jailani A, Lee JH, Ahmed B, Lee J. The antibiofilm effects of antimony tin oxide nanoparticles against polymicrobial biofilms of uropathogenic *Escherichia coli* and *Staphylococcus aureus*. Pharmaceutics 2023;15:1679.
42. Rodrigues AS, Batista JG, Rodrigues MÁ, Thipe VC, Minarini LA, Lopes PS, et al. Advances in silver nanoparticles: a comprehensive review on their potential as antimicrobial agents and their mechanisms of action elucidated by proteomics. Front Microbiol 2024;15:1440065.
43. Cheng J, Zhang H, Lu K, Zou Y, Jia D, Yang H, et al. Bi-functional quercetin/copper nanoparticles integrating bactericidal and anti-quorum sensing properties for preventing the formation of biofilms. Biomater Sci 2024;12:1788–800.
44. Zarenezhad E, Abdulabbas HT, Marzi M, Ghazy E, Ekrahi M, Pezeshki B, et al. Nickel nanoparticles: applications and antimicrobial role against methicillin-resistant *Staphylococcus aureus* infections. Antibiotics 2022; 11:1208.
45. Saleh MM, Refa't AS, Latif HKA, Abbas HA, Askoura M. Zinc oxide nanoparticles inhibits quorum sensing and virulence in *Pseudomonas aeruginosa*. Afr Health Sci 2019;19:2043–55.
46. Das P, Ghosh S, Nayak B. Phyto-fabricated nanoparticles and their anti-biofilm activity: progress and current status. Front Nanotechnol 2021;3: 739286.

Supplementary Material: This article contains supplementary material (https://doi.org/10.1515/ntrev-2025-0281).